Modeling Magnetic Field in Heavy ion Collisions Using Two Different Nuclear Charge Density Distributions

Susan Abbas Nejad

Supervisor: Dr. Umut Gürsoy

August 2017

Abstract

By studying the properties of matter during heavy-ion collisions, a better understanding of the Quark-Gluon plasma is possible. One of the main areas of this study, is the calculation of the magnetic field, how the values of conductivity effects this field and how the field strength changes with proper time. In matching theoretical calculations with results obtained in lab, two different models for charge density inside ions is used. In this thesis, after explanation of some theoretical background, the magnetic field contribution of the spectators and participants in Pb-Pb ion collision is calculated in a conductive medium and vacuum. Results are compared using the two different nuclear charge density models.

Keywords: Quark-Gluon Plasma, QCD, Heavy Ion Collisions, Electromagnetic field, Nuclear density distributions,

"Science is different to all the other systems of thought... because you don't need faith in it, you can check that it works."

— Brian Cox

Contents

1 Set-up of the problem

1.1 Introduction

One of the main areas of modern theoretical Physics is the theory of Quantum Chromodynamics (QCD for short). This theory studies the strong force which mainly acts between quarks and gluons. As the name suggests, this plasma is a soup of quarks and gluons. As predicted by this theory, matter at high energy changes into a quark gluon plasma phase. Some theories state that the universe was in this state in the "Quark Epoch", 10^{-12} until 10^{-6} seconds after the big bang [1]. This is also most likely the state of matter at the core of neutron stars [6]. This phase of matter is, thus, very interesting to study.

Since this phase transition is obtained at very high temperatures (thus high energies as well), it can only be obtained on Earth in laboratories like CERN (see figure 1 for a depiction of these experiments). At CERN, this state of matter is obtained by colliding lead ions together at near the speed of light with the nuclei having energies of a few trillion electron-volts each [14]. When two ions are collided together at very high speed, the result will be quark-Gluon plasma (QGP for short) formation for a short period of time (A sketch of the collision is shown in figure 1). Creating this phase of matter at these laboratories helps to study the structure of hadrons at high energy and how the QGP is thermalized. One of the steps in studying this medium is the study of its electromagnetic field. This thesis will focus on the magnetic field in such a collision using two different models describing the nucleon density.

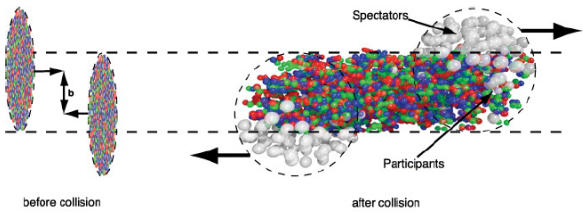

Figure 1: The set-up of a heavy-ion collision

Before describing the theory, it is useful to mention some characteristics of heavy-ion collisions:

1) One of the characteristics of a heavy-ion collision is its centrality. Collisions are mostly not head-on. Figure 1 again shows a sketch of an off-central collision. The center-to-center distance of the two ions is denoted by b. This constant expresses the level of centrality of the collision.

2) As the two ions are travelling at 99.9999 percent the speed of light [3], the ions will be strongly Lorentz contracted (contracted to 1 percent of their original size. See [12]). As a result, in this paper we assume that the neutrons and protons reside on a flat disk as this is an appropriate simplifying approximation.

3) As the collision is not head-on, there are two parts to the collision: the participants (participating in the collision) and the spectators (not participating in the collision) [2]. As seen in figure 2 bellow, the participant part of the collision is the area where the two circles

meet and the spectators reside on the rest of the are of the two circles (representing ions). In modeling the magnetic field of this plasma, we differentiate between these two part for reasons which shall be explained. We shall also compare their contribution to the total magnitude of the field. The calculated magnetic field in this thesis will be an interpolated function of proper time. Thus, we will also see how this field changes with time.

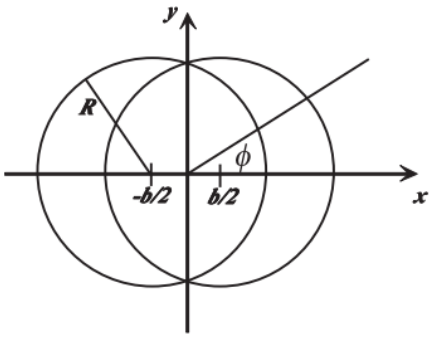

Figure 2: Sketch of an off-central collision. For the spectators one integrates over the two crescent-shaped parts of the two ions and for the participants, one integrates over the almond shaped part in the middle and accounting for both the ion moving in the +z direction and -z direction

1.2 A note on variables and constants

Before moving on any further, it is helpful to express some points about the variables. In this paper we choose a system of units in which the constants $\hbar = c = 1$. This system is called the Natural Units and is most commonly used in high energy Physics. Taking these constants as 1, we will have mass (m), momentum (mc), and energy (mc^2) units in GeV and units of length and time by GeV^{-1}. It is yet easier to work with a simpler unit by the Fermi length: $1fermi := 1fm = 10^{-15}m = 5.07GeV^{-1} = 3.33 \times 10^{-23}sec$ and $197MeV = 1fm^{-1}$.

As for the constants used in this thesis, we shall use the constants obtained by measurements taken at the Pb-Pb collision experiments at CERN which started in 2010 [18].

1.3 The electromagnetic fields for a single charged particle

1.3.1 The case where the particle is in a vacuum

To compute these fields, we proceed in steps. First we consider a single charged particle moving in the +z direction in vacuum. In the very early stage, the medium is assumed to be gluon dominated, such that the electric conductivity can be neglected (being roughly proportional to the sum of the electric charges squared, weighted by the densities of the charge-carrying species [9]). In the rest frame of that particle, there is no B field (charge is not moving) and thus the E field is:

$$\overrightarrow{E} = \frac{1}{4\pi\epsilon_0}\frac{q}{r^2}\hat{r}$$

To find the field in the lab frame, we can Lorentz transform the fields in the rest frame as follows:

$$F^{\mu\nu} = \begin{bmatrix} 0 & -E_1 & -E_2 & -E_3 \\ E_1 & 0 & -B_3 & B_2 \\ E_2 & B_3 & 0 & -B_1 \\ E_3 & -B_2 & B_1 & 0 \end{bmatrix}$$

With

$$\Gamma^{\mu}_{\nu} = \begin{bmatrix} \lambda & 0 & 0 & -\beta\lambda \\ 0 & 1 & 0 & 0 \\ 0 & 0 & 01 & 0 \\ -\beta\lambda & 0 & 0 & \lambda \end{bmatrix}$$

Where $F^{\mu\nu}$ is the Lorentz force and Γ^{μ}_{ν} is the Lorentz transformation tensor. Thus the transformed fields will be:

$$\begin{aligned} E'_1 &= \lambda(E_1 - \beta B_2) & E'_2 &= \lambda(E_2 + \beta B_1) & E'_3 &= E_3 \\ B'_1 &= \lambda(B_1 + \beta E_2) & B'_2 &= \lambda(B_2 - \beta E_1) & B'_3 &= B_3 \end{aligned} \tag{1.1}$$

Since in the rest frame we don't have any magnetic fields, B_x, B_y and B_z are zero. So we have:

$$E'_z = E_z = e\frac{\lambda(z-vt)}{([\lambda^2(z-vt)+y^2+z^2]^{1/2})^3} = e(1-\beta^2)\frac{(z-vt)}{[(z-vt)^2+(1-\beta^2)(y^2+x^2))]^{3/2}}$$
$$E'_y = e(1-\beta^2)\frac{y}{[(z-vt)^2+(1-\beta^2)(y^2+x^2))]^{3/2}}$$
$$E'_x = e(1-\beta^2)\frac{x}{[(z-vt)^2+(1-\beta^2)(y^2+x^2))]^{3/2}}$$

So the total electric field will be:

$$E = e(1-\beta^2)\frac{x+y+(z-vt)}{[(z-vt)^2+(1-\beta^2)(y^2+x^2))]^{3/2}}$$

This equation can be rewritten in terms of R and θ:

$$R = (z-vt)e_z + x + y$$

$$|R| = ((z-vt)^2+x^2+y^2)^{1/2}(z-vt)^2+(1-\beta^2)(x^2+y^2) = (1-\beta^2 Sin\theta^2)((z-vt)^2+x^2+y^2)$$

Setting $c = 1$ and simplifying the terms the electric and magnetic fields will become:

$$eE = \frac{1}{4\pi\epsilon_0}\frac{e^2}{\hbar c}\frac{(1-v_\alpha^2)R_\alpha}{(1-v_\alpha^2 Sin_\theta^2)^{3/2}R_\alpha^3}$$

$$eE_{tot} = \Sigma_\alpha \frac{(1-v_\alpha^2)R_\alpha}{(1-v_\alpha^2 Sin\theta^2)^{3/2}|R_\alpha|^3}$$

And

$$eB_{tot} = e(v_\alpha^2 \times E_t ot) = \Sigma_\alpha \frac{(1-v_\alpha^2)(v_\alpha \times R_\alpha)}{(1-v_\alpha^2 Sin\theta^2)^{3/2}|R_\alpha|^3}$$

1.3.2 The electromagnetic field of one charge in conductive environment

As for the conductivity value, according to [16], the following model is an accepted one for conductivity:

$$(5.8 + 2.9)\frac{T}{T_c}/197$$

Where T is plasma temperature and T_c is the critical temperature. This is the temperature at which hadrons start being produced from the QGP. Immediately after the collision, the plasma starts cooling down and at a certain moment it reaches a temperature cool enough for hadrons to be produced which is exactly this critical temperature. We take the value for this temperature to be 170 MeV 16. Thus, according to this model the value of conductivity is around 0.0663 at maximum and 0.0221 at minimum.

Up to now, we got the expressions for the fields in vacuum. However, the environment around a quark gluon plasma has a certain conductivity. As we shall see, this conductivity is such that it is negligible a very short time after the collision but it will effect the magnetic field a very short while afterwards (perhaps as the value of conductivity itself increases).

To find the expression for the Electromagnetic fields in this case, we first have to look at Maxwell's equations with conductivity included:

$$\begin{aligned}
&\nabla \cdot B = 0 \\
&\nabla \times E = -\frac{\partial B}{\partial t} \\
&\nabla \cdot E = 4\pi\rho \\
&\nabla \times B = (4\pi j + \frac{\partial E}{\partial t}) = \sigma E + e\upsilon\hat{z}\delta_{(}z - \upsilon t)\upsilon_{(}x_\perp \vec{-} \vec{x'_\perp}) + \frac{\partial E}{\partial t}
\end{aligned}$$

Here, we shall first find the expression for the magnetic field. Knowing the magnetic field at any point in space will also give us the electric field at that point (see formula 1.4).

With vectors we have the property:

$$\vec{A} \times (\vec{B} \times \vec{C}) = \vec{B}(\vec{A} \cdot \vec{C}) - \vec{C}(\vec{A} \cdot \vec{B})$$

So in our case we have:

$$\nabla \times (\nabla \times \vec{B}) = \nabla(\nabla \cdot \vec{B}) - \nabla^2\vec{B} = \frac{\partial(\nabla \times \vec{E})}{\partial t} + \sigma(\nabla \times \vec{E}) + e\upsilon(\nabla \times \vec{Z})$$

Where:

$$Z = \hat{z}\delta_{(z-\upsilon t)}\upsilon_{(\vec{x_\perp} - \vec{x'_\perp})}$$

Replacing expressions from Maxwell's equations and the expression for Z, we get the equation for the magnetic field:

$$\nabla^2\vec{B} - \frac{\partial^2\vec{B}}{\partial t^2} - \sigma\frac{\partial\vec{B}}{\partial t} = -e\upsilon\vec{\nabla}\times(\hat{z}\delta_{(z-\upsilon t)}\delta_{(x_\perp - x_\perp)})$$

Since the differential operators here are linear, we can use the method of Green's function to solve for B. In general, for these types of problems one has:

$$Lu_{(x)} = f_{(x)} \tag{1.2}$$

Where L is a linear differential operator and $u_{(x)}$ is the function we are going to find the expression for. Green's function for the operator L is a function which satisfies:

$$LG_{(x,s)} = \delta_{(x-s)} \tag{1.3}$$

Multiplying both sides of eq. 1.3 by f_x and integrating we get:

$$\int LG_{(x,s)}f_s d_s = \int \delta_{(x-s)}f_{(s)}d_s = L\int G_{(x,s)}f_s d_s = f_{(x)} = Lu_{(x)}$$

So:

$$u_{(x)} = \int G_{(x,s)}f_s d_s$$

In our case $u_{(x)} = B_{(z,b,t)}$. The function f is:

$$f_{(z,b,t')} = -e\upsilon\vec{\nabla}\times(\hat{z}\delta_{(\vec{z'}-\upsilon t')}\delta_{(\vec{b'})})$$

Again, since we are finding the expressions for the fields in terms of variables in lab frame (primed variables), we use those variables in our formulas as well.

For simplicity we can take $b = x_\perp - x_\perp{}'$ So the magnetic field in terms of G is:

$$\vec{B}_{(z,b,t)} = \int_z\int_{\vec{b}}\int_t G_{(z-z',b-b',t-t')}e\upsilon\vec{\nabla}\times(\hat{z}\delta_{(\vec{z'}-\upsilon t')}\delta_{(\vec{b'})})d^2_{b'}d_{z'}d_t$$

To find G, we go back to the definition (1.2):

$$\nabla^2\vec{G} - \frac{\partial^2\vec{G}}{\partial t^2} - \sigma\frac{\partial\vec{G}}{\partial t} = -\delta_{(z-z')}\delta_{(\vec{b}-\vec{b'})}\delta_{(t-t')} \tag{1.4}$$

Now we shall use the Fourier transform of G because for the F-transform of a function f we have:

$$F(f'_{(x)}) = ixF(f_{(x)})$$

The F-transforms are:

$$G_{(kz,\vec{b},t,z',\vec{b'},t')} = \int_{-\infty}^{\infty} G_{(z,\vec{b},t,z',\vec{b'},t')}e^{-ik_z z}d_z$$

$$G_{(kz,\vec{k}_\perp,t,z',\vec{k'}_\perp,t')} = \int_{-\infty}^{\infty} G_{(z,\vec{b},t,z',\vec{b'},t')}e^{-i\vec{k}_\perp\dot{b}}d^2_{\vec{b}}$$

$$G_{(kz,\vec{b},\omega,z',\vec{b}',\omega')} = \int_{-\infty}^{\infty} G_{(z,\vec{b},t,z',\vec{b}',t')} e^{i\omega t} d_t$$

Where:

$$\vec{k} = k_z\hat{z} + \vec{k_\perp}$$

$$\begin{aligned}\vec{\nabla^2 G_f} - \frac{\partial^2 G_f}{\partial t^2} - \sigma\frac{\partial \vec{G}_f}{\partial t} &= -(k_z^2 + k_\perp^2)G_f + \omega^2 G_f + i\sigma\omega G_f \\ &= G_f[-k_z^2 - k_\perp^2 + \omega^2 + i\sigma\omega]\end{aligned}$$

Since we have:

$$F_x(\delta_{(x-x_0)} = \int_{-\infty}^{\infty} \delta_{(x-x_0)} e^{-ikx} d_x d_x = e^{-ikx_0}$$

So expression 1.4 becomes:

$$\vec{\nabla^2 G_f} - \frac{\partial^2 G_f}{\partial t^2} - \sigma\frac{\partial \vec{G}_f}{\partial t} = -(e^{-ik_z z'} e^{-i\vec{k}_\perp \dot{b}'} e^{i\omega t'})$$

So the transform of G is:

$$G_{f(k_z,\vec{k}_\perp,\omega)} = \frac{e^{-ik_z z'} e^{-i\vec{k}_\perp \dot{b}'} e^{i\omega t'}}{k_z + k_\perp - \omega^2 - i\sigma\omega}$$

Using inverse F-transform we get G:

$$G_{(z-z',b-b',t-t')} = \iiint_{-\infty}^{\infty} (\frac{1}{k_z + k_\perp - \omega^2 - i\sigma\omega})[\frac{1}{2\pi} e^{ik_z(z-z')}][(\frac{1}{2\pi})^2 e^{ik_\perp(b-b')}][\frac{1}{2\pi} e^{-i\omega(t-t')}] d_{k2} d_{k\perp}^2 d_\omega \tag{1.5}$$

For Z we have:

$$\vec{\nabla} \times Z = \vec{\nabla} \times (\hat{z}\delta_{(z'-\upsilon t')}\delta_{(\vec{b'})}) = \delta_{(z'-\upsilon t')}(\delta_y \delta_{(\vec{b'})}, \delta_x \delta_{(\vec{b'})}, 0) \tag{1.6}$$

Putting expressions 1.5 and 1.6 in the expression for B we get:

$$B_{(z,\vec{b},t)} = 2\pi e\upsilon \int \frac{{d_{k\perp}}^2}{(2\pi)^2} e^{(i\vec{b}k_\perp)} \int \frac{d_{kz}}{2\pi} e^{ik_z z} \int \frac{d\omega}{2\pi} e^{(-i\omega t)} \frac{(i\vec{k} \times \hat{z})\delta_{(\omega - k_z\upsilon)}}{k_z^2 + k_\perp^2 - \omega^2 - i\sigma\omega}$$

From here onward it is convenient to find expressions for B_x, B_y and B_z separately. For the y-component we have:

$$(\vec{k_\perp} \times \hat{z}) \cdot \hat{y} = -k_x = -k_\perp Cos_{(\phi)}$$

For the x-component:

$$(\vec{k_\perp} \times \hat{z}) \cdot \hat{x} = -k_x = -k_\perp Sin_{(\phi)}$$

For the z-component:

$$(\vec{k_\perp} \times \hat{z}) \cdot \hat{z} = 0$$

However, in the center of the system (where we finally plot the B field), the x-component is also not contributing 13 and thus the only component to study is the y-component of the field:

$$\vec{B_y} = e\hat{y} \int\int \frac{1}{(2\pi)^2} \frac{-ik_\perp cos(\varphi)}{(\omega/\upsilon)^2 + k_\perp^2 - \omega^2 - i\sigma\omega} e^{-ibk_\perp cos(\varphi)} e^{i\omega(\frac{z}{\upsilon} - t)} d_{k_\perp}^2 d_\omega$$

For $d_{k_\perp}^2$ we have:

$$d_{k_\perp}^2 = k_\perp dk_\perp d\phi$$

So:

$$B_y = e\hat{y} \int\int\int \frac{1}{(2\pi)^2} \frac{-ik_\perp^2 cos(\varphi)}{(\omega/\upsilon)^2 + k_\perp^2 - \omega^2 - i\sigma\omega} e^{-ibk_\perp cos(\varphi)} e^{i\omega(\frac{z}{\upsilon} - t)} d_{k\perp} d_\omega d_\varphi$$

The omega part of the integral can be calculated analytically:

$$\int -ik_\perp Cos(\varphi) e^{(-ibk_\perp cos(\varphi) d_\varphi)} d_\varphi = \frac{d}{db} \int e^{(-ik_\perp b cos(\varphi))} d_\varphi \tag{1.7}$$

$$\int e^{(-ik_\perp b cos(\varphi))} d_\varphi = \int e^{(-ibk_\perp cos(\varphi))} d_\varphi = 2\pi J_0(bk_\perp)$$

Where J_0 is the Bessel function. So the right hand side of the equation 1.7 will be:

$$2\pi \frac{d}{db}(J_0(bk_\perp)) = 2\pi k_\perp J_1(bk_\perp)$$

And the B field becomes:

$$eB_y = 2^{\alpha_{em}} \hat{y} \int\int \frac{J_1(bk_\perp) k_\perp^2}{\frac{\omega^2}{\upsilon^2} + k_\perp^2 - \omega^2 - i\sigma\omega} e^{i\omega(\frac{z}{\upsilon} - t)} d_{k\perp} d_\omega$$

Here, as the particle is moving at a speed very close to the speed of light, we can make the simplifying assumption that $\upsilon = c = 1$. In this case the magnetic field will be:

$$eB_y = 2\alpha_{em} \hat{y} \int\int \frac{J_1(bk_\perp) k_\perp^2}{k_\perp^2 - i\sigma\omega} e^{i\omega(z-t)} d_{k\perp} d_\omega$$

From here we proceed first by solving the integral over omega. This integral can be solved using the residue theorem from complex analysis. According to this theorem, the integral of a function over a closed curve is:

$$\int f_{(z)} d_z = 2\pi i \Sigma Res(f, a_k)$$

Where a_k are the poles of the function. Here there is only one pole at $\frac{k_\perp^2}{i\sigma} = \omega$. So we get:

$$\int \frac{e^{(i\omega(z-t))}}{i\sigma(\frac{k_\perp^2}{i\sigma}-\omega)}d_\omega = 2\pi i\Sigma Res(f, a_k = \frac{k_\perp^2}{i\sigma})$$

Where the residue is:

$$\text{Res(f,a}_k = \tfrac{k_\perp^2}{i\sigma}) = Lim \underset{\omega \frac{k_\perp^2}{i\sigma}}{\rightarrow} \frac{e^{i\omega(z-t)}}{i\sigma} = \tfrac{1}{i\omega} e^{i\frac{k_\perp^2}{i\sigma}(z-t)}$$

So the integral becomes:

$$eB_y = \frac{4\pi\alpha_{em}}{\sigma}\hat{y}\int J_1(bk_\perp)e^{\frac{k_\perp^2}{\sigma}(z-t)}k_\perp^2 dk_\perp$$

The integral over $k_\perp$ can be evaluated analytically:

$$eB_y = \hat{y}\frac{\alpha_{em}b\sigma}{2(t-z)^2}e^{\frac{b^2}{e^{4(t-z)}}}$$

However, for a more accurate calculation, we take $\upsilon \neq 1$. Thus in this case we have:

$$eB_y = \frac{\alpha_{em}}{\pi}\hat{y}\int J_1(bk_\perp){k_\perp}^2 dk_\perp \int \frac{e^{i\omega(\frac{z}{\upsilon}-t)}}{\frac{\omega^2}{\upsilon^2}+k_\perp^2-\omega^2-i\sigma\omega}d\omega$$

$$eB_y = \frac{\alpha_{em}}{\pi}\hat{y}\int J_1(bk_\perp)k_\perp^2 d_{k\perp} \int \frac{e^{i\omega(\frac{z}{\upsilon}-t)}}{\frac{\omega^2}{\upsilon^2}+k_\perp^2-\omega^2-i\sigma\omega}d_\omega$$

In this case we have two poles:

$$\omega_\pm = \frac{i\sigma\lambda^2\upsilon^2}{2}(1 \pm \sqrt{1+\frac{4k_\perp^2}{\sigma^2\lambda^2\upsilon^2}})$$

Here, we pick only the ω_- part as with the other one, the function for B would diverge. Picking ω_- and calculating the residue for this pole; we get for the field:

$$eB_y = \frac{\alpha_{em}}{\pi}\hat{y}\int \frac{J_1(bk_\perp)k_\perp^2 e^{(-\omega_-(\frac{z}{\upsilon}-t))}}{\sigma(1+\frac{4{k_\perp}^2}{\sigma^2\lambda^2\upsilon^2})^{1/2}}d_{k\perp}$$

To calculate the integral we first change the variables in the following way:

$$u = (1+\frac{4{k_\perp}^2}{\sigma^2\lambda^2\upsilon^2})^{1/2}$$

$$\frac{du}{dk_\perp} = \frac{1}{u}\frac{4k_\perp}{\sigma^2\lambda^2\upsilon^2}$$

$$u^2 - 1 = \frac{4{k_\perp}^2}{\sigma^2\lambda^2\upsilon^2}$$

$$k_\perp = \frac{\sigma\lambda\upsilon}{2}\sqrt{u^2-1}$$

$$dk_\perp = u(\frac{\sigma^2\lambda^2\upsilon^2}{4k_\perp})du$$

So the field becomes:

$$eB_y = \frac{\alpha_{em}}{\pi}\hat{y}\int \frac{2J_1\frac{b\sigma\lambda\upsilon}{2}\sqrt{u^2-1}(\frac{\sigma^2\lambda^2\upsilon^2}{4})^2\sqrt{u^2-1}}{\sigma^2\lambda\upsilon}e^{-\frac{\sigma\lambda^2\upsilon^2}{2}(1-u)(t-\frac{z}{\upsilon})}du$$

Putting the constant terms to the left side of the integral:

$$eB_y = \frac{\alpha_{em}}{2\pi}[\frac{b\sigma^3\lambda^4\upsilon^4}{8}e^{-\frac{\sigma\lambda^2\upsilon^2}{2}(t-\frac{z}{\upsilon})}]\int J_1(\frac{b\sigma\lambda\upsilon}{2}\sqrt{u^2-1})\sqrt{u^2-1}e^{-\frac{\sigma\lambda^2\upsilon^2}{2}(t-\frac{z}{\upsilon})u}du$$

This integral can again be calculated analytically:

$$eB_y = \frac{2\pi(\lambda^2\sigma^2\upsilon^2)}{4}\frac{\lambda\upsilon}{2}e^{(t-\frac{z}{\upsilon})\frac{\sigma\lambda^2\upsilon^2}{2}}\sqrt{\frac{2}{\pi}}\beta(\alpha^2+\beta^2)^{-3/4}K_{3/2}(\sqrt{\alpha^2+\beta^2})$$

Where

$$K_{3/2}(z) = \frac{2}{\pi}e^{-z(1+\frac{1}{z})}$$

1.4 Coordinate transformations:

Now we have the B field in terms of the normal variables (x, y, z, t) and v. However, there is a more convenient coordinate system to describe heavy ion collisions. That system uses τ (proper time) , η (pseudo-rapidity) , $x_\perp$ (distance from the center of the ion to where we want to find the field) and ϕ (angel from x axes to the line of $x_\perp$).

Pseudo-rapidity in natural units is a dimension-less coordinate which is similar to a hyperbolic angel [18]. In this system of coordinates, instead of using speed, we use a similar constant related to speed called rapidity Y. These variables are the experimental observables in heavy ion collision experiments and thus are more convenient to work with [7]. The transformations from Cartesian coordinates to the new coordinates are as follows:

$$\tau = \sqrt{t^2-z^2} \qquad \eta = arctanh(\frac{z}{t}) \qquad x_\perp = \sqrt{x^2+y^2}$$

$$\varphi = acrtan(y/x) \qquad Y = arctanh(\frac{\upsilon_z}{C}) \qquad z' = \beta t$$

And the other way:

$$t = \tau Cosh(\eta) \qquad x = x_\perp Cos(\varphi) \qquad y = x_\perp Sin(\varphi)$$
$$z = \tau sinh(\nu) \qquad \upsilon = tanh(Y)$$

At this stage one should consider taking into account the correct range for the variables. As it can be seen, $\eta = 0$ corresponds to the t-axis and $\eta = \pm\infty$ corresponds to the light cone ($z = t$). As the results do not depend on the pesudo-rapidity window in which we initialize the particles (as long as it is larger than the observed rapidity bins), for most studies, the ammount $-3 < \eta < 3$ is sufficient [9]. This value is also within the window of pseudo-rapidity calculations in ALICE [4]. For rapidity, we also use the value $Y_0 \simeq 7.6$ used in the LHC experiments [10]. As for τ, we use the proper time until the time of thermalization. It is known that the proper time of thermalization is about 0.5 fm [15].

The magnetic field in terms of the new variables is:

$$eB_y^+(\tau, \eta, x_\perp, \phi) = \alpha \sinh(Y_b)(x_\perp \cos\phi - x'_\perp \cos\phi') \frac{(\frac{|\sinh(Y_b)|}{2}\sqrt{\Delta} + 1)}{\Delta^{\frac{3}{2}}} e^A \,,$$

where $\alpha = e^2/(4\pi)$ is the electromagnetic coupling constant, $Y_b \equiv \text{arctanh}(\beta)$ is the rapidity of the particle moving in the +z direction. We have also defined:

$$A = \frac{\sigma}{2}(\tau \sinh(Y_b)\sinh(Y_b - \eta) - |\sinh(Y_b)|\sqrt{\Delta}$$

$$\Delta = \tau^2 \sinh^2(Y_b - \eta) + {x_\perp}^2 + (x'_\perp)^2 - 2 \times x_\perp \times x'_\perp \times \cos(\phi - \phi')$$

We only take into account the y component of the field since we will be studying the field evolution at around the center where this component is the main component of the field as also stated by [12]. Knowing the Magnetic field, one can find the Electric field as follows:

$$eE_x^+(\tau, \eta, x_\perp, \phi) = eB_y^+(\tau, \eta, x_\perp, \phi) \coth(Y_b - \eta) \,. \tag{1.4}$$

So now we have the x,y and z part of the Electric and magnetic field for one moving particle in lab frame (calculations also carried out by [10 , 16]).

2 Numerical Integration

At this stage, we have the contribution to the magnetic field for only one particle. our aim is to integrate over the contributions of the field from all the particles on the 2D ion discs (see figure 2).

As we will see later, the integral, when found, will be a function of $(\eta, \tau, \phi, x_\perp)$. This integral cannot be found analytically as it is too complicated. Hence, we use numerical integration to find a good approximation to the integral.

In this section we discuss the assumptions and models used to do this integration. First, two different models for particle distribution functions inside the ions are introduced. Afterwards some theories regarding relations with proper time are discussed. Afterwards, the magnetic field is calculated using the two models for and the results are compared.

2.1 two different nuclear Distribution Function models

To find the magnetic field of the moving ion, we have to add up the contributions due to all the particles (see figure 1). For this purpose, we use two different models for distribution of protons inside the nuclei. As we shall see, the hard-sphere distribution is more simplified than the Woods-Saxon distribution which may be unrealistic in some situations. Thus, in following the numerical calculation of the magnetic field, we use both these distributions to compare them with previously obtained results.

2.1.1 The Woods-Saxon model

The more accurate of the two nuclear Distribution Function models is called the Woods-Saxon model where the number density of protons is given by the equation bellow (see also [5] and [10]):

$$n_A(r) = \frac{n_0}{1 + e^{\frac{r-R}{d}}} \tag{2.1}$$

Where R is the radius of the nuclei and r is the distance from the center of nuclei. The values for constants are $n_0 = 0.17fm^{-1}$ and $d = 0.54fm$ and $R = 7fm$. The distance from the center of nuclei in terms of the x-y-z coordinates is:

$$r_\pm = \sqrt{(x \pm \frac{b}{2})^2 + y^2 + z^2}$$

Switching to the new coordinate system:

$$r_\pm = \sqrt{(x'_\perp \pm bx'_\perp Cos(\phi')) + \frac{b^2}{4} + (z - \tau^2 Sinh^2(\eta))}$$

The figures 3 and 4 show some plots of the number density function (2.1):

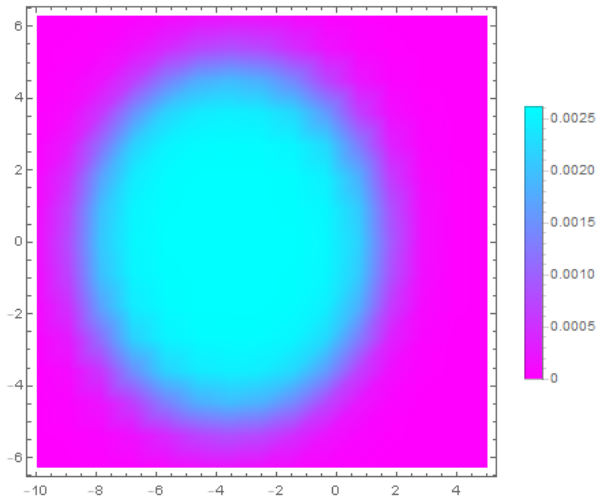

Figure 3: Plot of the number density function (equation 2.1) for Woods-Saxon model in terms of x and y for lead ion the center of which is positioned at $x_{\perp 0} = 3.5$. The Plot-Legend on the right shows the relative value for the number density function for the corresponding colour. As we can see here, the density is highest at the center and lowest as we go to the borders of the ion as expected.

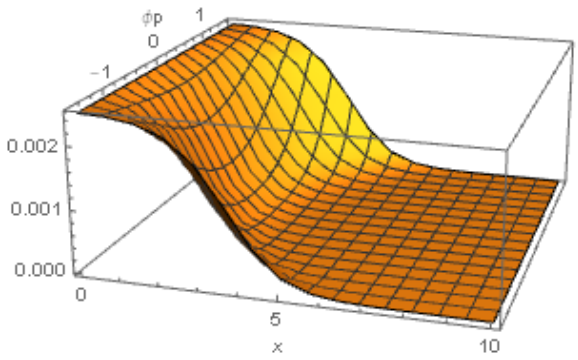

Figure 4: 3D plot of the number density as a function of $x'_\perp$ and ϕ'. It is visible that along a constang angel, as x increases, the number density decreases. This drop in density is similar to the drop in Woods-Saxon potential as a function of x; as expected.

To get the density at any ($x_\perp$, ϕp) we integrate over z (see the integral bellow). The reason for the original z-dependence is due to the uncertainty in the position of each particle along the z direction.

$$\rho_\pm(x'_\perp) = \frac{1}{N}\int dz' \frac{n_0}{1 + e^{\frac{r-R}{d}}} \tag{2.2}$$

Where N is the normalization factor. The values for constants are $n0 = 0.17fm^{-3}$ and $N = 1.6487$ and $d = 0.54fm$. This integral is also of the type which cannot be evaluated analytically and a numerical calculation must be done to evaluate a near-enough approximation. Figures 5 and 6 show the resulting density function.

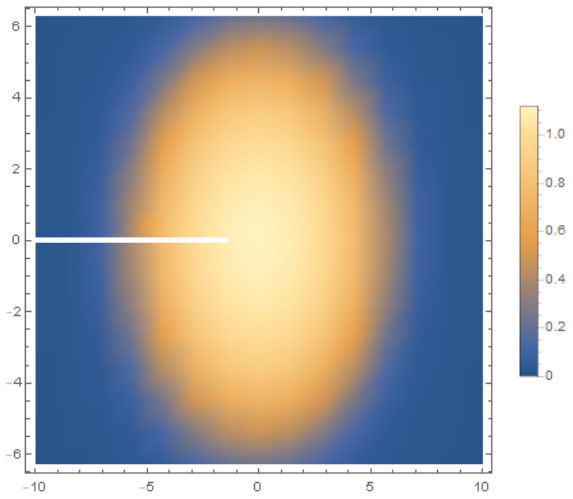

Figure 5: Density plot of the Integrated density function (equation 2.2) for Woods-Saxon model. The integral is approximated by numerical integration (see Appendix) and a function $\rho_{(x_\perp,\phi')}$ is obtained by interpolation.

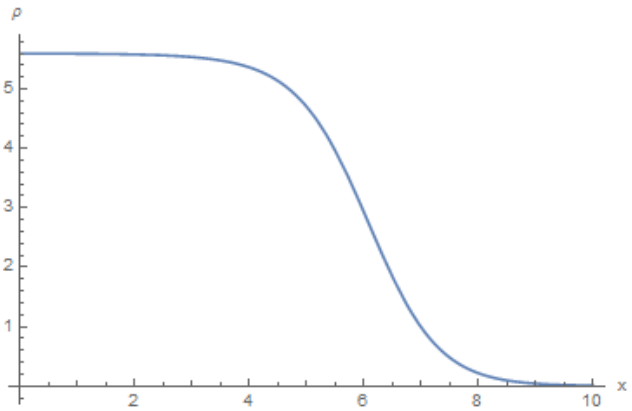

Figure 6: 2D plot of the interpolation function that shows the drop in the density as x increases from the center to the border of the ion.

2.1.2 Hard-Sphere model

Another model for the density function of charges within an ion is the Hard-Sphere model which is more simplified and easier to work with:

$$\rho_{\pm}(x'_{\perp}) = \frac{3}{2\pi R^3}\sqrt{R^2 - (x'_{\perp} \pm bx'_{\perp}Cos(\phi')) + \frac{b^2}{4}} \tag{2.3}$$

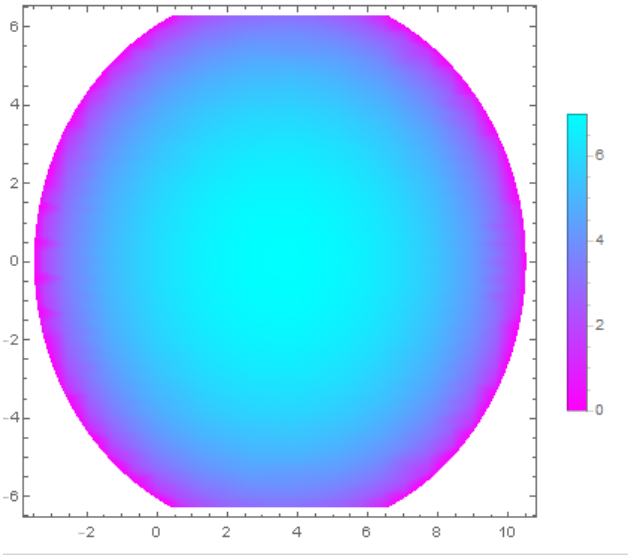

Figure 7: the density-plot of the density function for Hard-Sphere model in terms of x and y for lead ion. The Plot-Legend on the right show the relative value for the density function for the corresponding colour. It is observed that the density is highest at the center and lowest as we go to the borders, exactly as one would expect to get with a sphere of uniformly distributed matter. However, as this model is more simplified, it also looks more symmetric and perfect which may be an unrealistic model in some situations.

2.2 A note on Proper Time

One way to follow the numerical integration is to do so on the freeze-out surface. This surface is a hyper-surface in space-time where hadrons are produced during the collision as the matter cools down which is defined by a function $\tau_{freeze[x_\perp]}$ [18]. Calculation of the magnetic field on this surface decreases the number of variables by one.

Another way, however, is to integrate for the magnetic field at any point in space-time and not just the freeze-out surface. This way requires more computation time; but is more accurate.

2.3 Spectator contribution

At this point one has to differentiate between the spectators and the participants when doing the numerical integration. For the spectator contribution, the amount of rapidity does not change (the particles are not participating in any reaction and are assumed to move with constant speed before and after the collision), but for the participants it does change. In our case for Pb-Pb collisions with center-of-mass energy per nucleon pair of about 2 TeV we take $Y0 \equiv 7.6$ [4]. For the spectator contribution, we only integrate over $x'_\perp$ and ϕ' as follows [10]:

$$\Sigma eB_{s,y} = -Z \int_{-\frac{\pi}{2}}^{\frac{\pi}{2}} d\phi' \int_{x_{in}}^{x_{out}} \rho_\pm(x'_\perp)\theta_\pm(x_\perp)(1-\theta_\mp(x_\perp))eB_i x_\perp dx'_\perp$$

Where $\rho_{\pm}(x'_{\perp})$ describes the particle distribution function for a relativistic ion and $\theta_{-(x_{\perp})} = \theta[R^2 - (x_{\perp} - \frac{b}{2}\hat{x})^2]$. We use $Z = 82$ as it is the atomic number for Lead nuclei which is used in heavy ion collisions at CERN. Here, x_{in} and x_{out} describe the crescent shaped loci where we find the particles which are either moving in the +z or -z direction but not both and are described by the following functions [10]:

$$x_{in/out}(\phi') = \mp\frac{b}{2}cos(\phi') + \sqrt{R^2 - \frac{b^2}{4}sin^2(\phi')}$$

The θ functions account for charges moving in the opposite directions. Replacing these functions by the magnetic field as a function of $\phi, \eta, x'_{\perp}, \tau$ (moving in +z direction) and $\pi - \phi, -\eta, x'_{\perp}, \tau$ (moving in -z direction) we get:

$$eB^{-}_{s,y} = -Z\int_{-\frac{\pi}{2}}^{\frac{\pi}{2}} d\phi' \int_{x_{in}}^{x_{out}} x'_{\perp}\rho_{+}(x'_{\perp})((eB^{+}_{y}(\pi - \phi, -\eta, x'_{\perp}, \tau)) + (eB^{+}_{y}(\phi, \eta, x'_{\perp}, \tau)))dx'_{\perp}$$

2.3.1 Spectator contribution with The Hard-Sphere model

For the particle distribution function, we first use the hard-sphere model which is easier to work with. This has been done before by [10] and is done here for comparison. The figures 8 and 9 and 10 bellow show the results of the numerical calculation using the density function shown in formula (2.3), with and without conductivity:

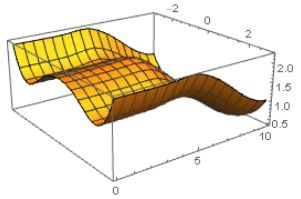

Figure 8: 3D plot of the B field in terms of (η , xp) at $\tau = 0.3$ and $\phi = \frac{\pi}{2}$ using the hard sphere distribution in medium with zero conductivity

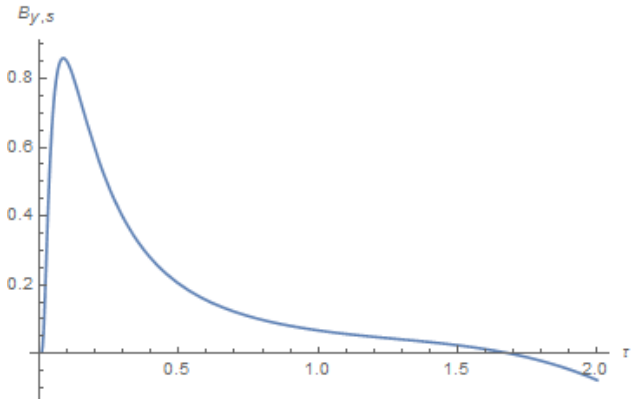

Figure 9: Plot of the interpolated function of total B field in terms of τ at ($xp = 0.001$, $\phi = \frac{\pi}{2}$, $\eta = 0.1$) in medium with zero conductivity. The maximum value of the field is $0.85fm^{-2}$ which, upon conversion gives us 1.7×10^{18} Gauss. As expected, results are similar to [10]. The part of the graph that is negative is a result of extrapolation and shall be ignored.

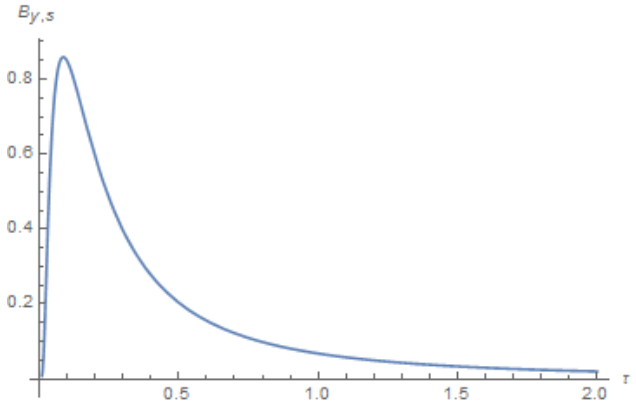

Figure 10: Plot of the interpolated function of B in terms of τ at ($xp = 0.001$, $\phi = \frac{\pi}{2}$, $\eta = 0.1$) with the exception of having non-zero conductivity ($\sigma = 0.023$). Again, results are similar enough to [10].

It is clear from the figure that the field is very strong at low values of τ . In the short moments before/during/after the impact of two ions in non-central collisions, there is a very strong magnetic field in the reaction zone [19]. In fact, being of order of 10^{18} Gauss, these fields are among the strongest magnetic fields in nature [9].

As can also be seen, these fields decay almost immediately (put the values in seconds). However, including the effects of a conducting medium, the field decays slower (see also [19] and figure 11 bellow).

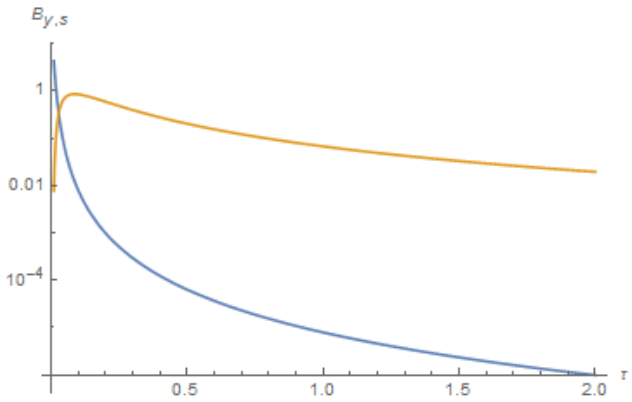

Figure 11: Figures 9 and 10 plotted together. the blue line shows the field without conductivity and the orange line shows the field including conductivity. As can be seen, a conductive medium slows down the decay of the magnetic field. In the very early times, the plot using a medium without conductivity is more accurate as the conducting medium is not formed immediately as quarks take some time to be created from the Glasma field 13. Also we assumed that the medium does not alter during the evolution of QGP, thus the usage of a constant value for conductivity. However, as also seen from the graph, a decrease in conductivity due to expansion of the medium will only increase the decay speed of the magnetic field [13].

2.3.2 Spectator contribution with Woods-Saxon Model

To calculate the field using this model, we use the function obtained by interpolation (described in section 2.1.1). Figure 12 bellow shows the obtained result with conductivity. The maximum value here is about $0.95 fm^{-2}$. Compared with the maximum value of about $0.84 fm^{-2}$ it shows a higher but close-enough value (see figure 13 bellow).

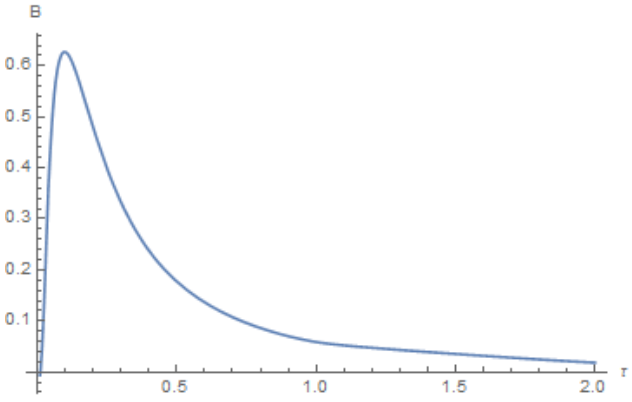

Figure 12: Spectator contribution to the magnetic field using Woods-Saxon Model in conductive medium

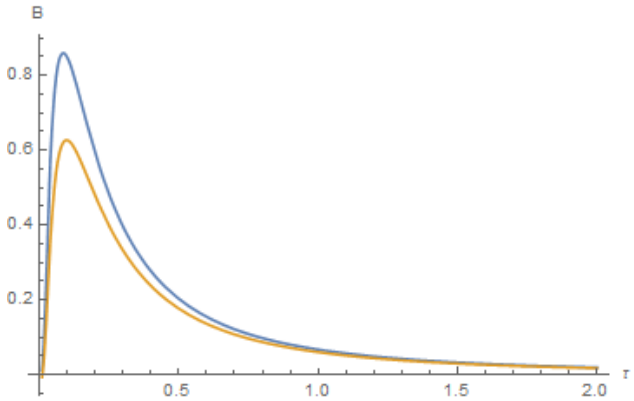

Figure 13: Spectator contribution using Woods-Saxon Model (orange) and Hard-Sphere (blue) plotted together. As seen, both are within the order of magnitude window of 10^{18} Gauss which, in the realm of the strong fields produced as a result of heavy ion collisions, is close enough.

2.3.3 Participants

Unlike the calculation of the B-field for Spectators where the rapidity Y does not change (because they do not collide with particles from the other direction), for the participant contribution to the field, we have to take into account the change in rapidity. Thus, to get the total field we will also integrate over the distribution of Y given by the equation bellow ([12] and [11]).

$$f(Y_b) = \frac{a}{2Sinh(aY_0)} e^{aY_b} \tag{2.4}$$

Where $-Y_0 < Y_b < Y_0$ [10] and $Y0 \approx 7.6$ and $a \approx 0.5$. Thus the total field will be 10:

$$eB_{y,p} = -Z \int_{-Y_0}^{Y_0} f(Y_b) d_{Y_b} \int_{-\frac{\pi}{2}}^{\frac{\pi}{2}} d\phi' \int_0^{x_{in}(\phi')} \rho_{\pm}(x'_{\perp}) \theta_{\pm}(x_{\perp})(1 - \theta_{\mp}(x_{\perp})) eB_i x_{\perp} dx_{\perp}$$

2.3.4 Participants contribution with The Hard-Sphere model

Figure 14 bellow shows the participants contribution to the Magnetic field using the Hard-Sphere model. As we can see, the maximum of the field is only about $0.065 fm^{-1}$, i.e. about only a hundredth of the contribution of the spectators. This is mainly due to the fact that there are less particles participating in the collision.

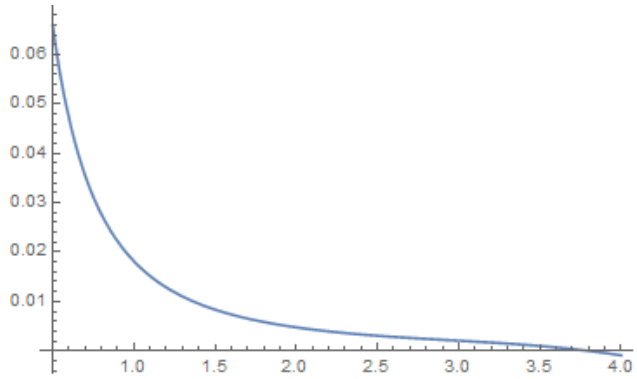

Figure 14: Plot of the proper-time dependence of participants part of eB_y

2.3.5 Participants contribution with Woods-Saxon Model

Figure 15 bellow shows the same contribution using the Woods-Saxon model. Again, the maximum value of the field is the same and about $0.065 fm^{-1}$ showing that the two models produce similar results in the case of the participants.

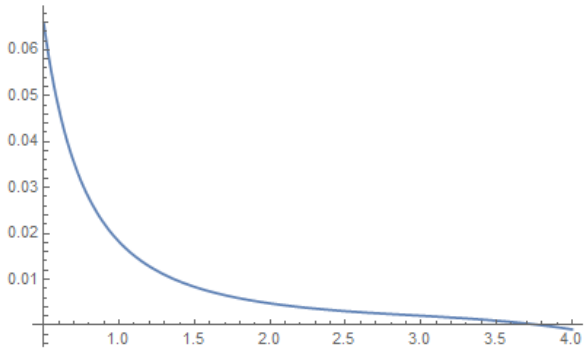

Figure 15: Plot of the proper-time dependence of the magnetic field of the participants using the Woods-Saxon model

3 Conclusion

In heavy-ion collisions, the nuclei pass each other at very high velocity. In these high energy situations, the confined matter inside the ions turns into the unconfined QGP. It is found that the relativistically moving heavy ions, typically with large positive charges, carry strong magnetic (and electric) fields with them. In the short moments before/during/after the impact of two ions in off-central collisions, there is a very strong magnetic field in the reaction zone. In fact, such a magnetic field is estimated to be of the order of 10^{18} Gauss, probably the strongest magnetic field in the present universe [8]. Since the distances between the nucleons are very small very close to the reaction time (and shortly afterwards), one would expect that the magnetic field of such reactions is very high. As argued by [17], observation of Lepton polarization can prove the existence of such strong fields in heavy-ion collision experiments.

In this thesis we employed a semi-analytical model taking relativistic heavy ions as two Lorentz-contracted spheres of charge densities described by two different models. Ignoring interactions of particles we have then compared the resulting magnetic field obtained as a function of proper time. In our results we obtained the spectator contribution to the field which at its maximum has the strength of about 1.7×10^{18} Gauss using the Hard-Sphere model and 1.2×10^{18} Gauss for the Woods-Saxon model. We have also shown that the contribution to the field from the participants is negligible and that taking into account the conductivity, the field decays much slower.

Finally, we have argued that our results using the Woods-Saxon model match; in order of magnitude and up to statistical fluctuations, to results obtained using the approximation of a homogeneously-charged sphere by [10 , 13]. Therefore, we conclude that due to its simplicity, the Hard-Sphere model for charge distribution is a good-enough approximation when calculating electromagnetic fields in heavy ion collisions.

4 Potential topics for Further research

As we have seen, an enormous magnetic field can indeed be created in off-central heavy-ion collisions. At this point, there are some useful adjustments to the model which could be topics of further research:

1) In finding a realistic value for the conductivity in relation to temperature, we assumed that the medium does not alter during the evolution of QGP, thus the usage of a constant value for conductivity. A case for study here would be to take into effect the quark contributions and the time-dependence of temperature (and thus the conductivity) on the model for the magnetic field [16].

2) As in this thesis all the calculations were done for the magnetic field, the same calculations can be simply done for the Electric field of the medium using relation 3.1.

3) We have seen that the magnitude of the created magnetic field drops as a function of proper time. This change in the magnetic field induces an electric field circulating around the direction of B_y by Faraday's Law. This electric field in turn creates a current which again induces an electric field in the z direction by the Lenz rule. Study of the effects of these inductions on the evolution of the colliding system is an interesting topic for further research (see also 17).

References

[1] J Allday. *Book Review: Quarks, leptons and the big bang.-/Institute of Physics, 2002.* 2002.

[2] *CERN COURIER Participants and spectators at the heavy-ion fireball.* `http://cerncourier.com/cws/article/cern/53089`. Accessed: 2017-07-20.

[3] *Cerncourier Kernel Description.* `http://cerncourier.com/cws/article/cern/53089`. Accessed: 2017-07-21.

[4] ALICE collaboration et al. "Centrality, rapidity and transverse momentum dependence of J/ψ suppression in Pb–Pb collisions at". In: *Physics Letters B* 734 (2014), pp. 314–327.

[5] CW De Jager, H De Vries, and C De Vries. "Nuclear charge-and magnetization-density-distribution parameters from elastic electron scattering". In: *Atomic data and nuclear data tables* 14.5-6 (1974), pp. 479–508.

[6] Robert C Duncan and Christopher Thompson. "Formation of very strongly magnetized neutron stars-Implications for gamma-ray bursts". In: *The Astrophysical Journal* 392 (1992), pp. L9–L13.

[7] Panagiota Foka and Małgorzata Anna Janik. "An overview of experimental results from ultra-relativistic heavy-ion collisions at the CERN LHC: bulk properties and dynamical evolution". In: *Reviews in Physics* 1 (2016), pp. 154–171.

[8] Dario Grasso and Hector R Rubinstein. "Magnetic fields in the early universe". In: *Physics Reports* 348.3 (2001), pp. 163–266.

[9] Moritz Greif, Carsten Greiner, and Zhe Xu. "Magnetic field influence on the early time dynamics of heavy-ion collisions". In: *arXiv preprint arXiv:1704.06505* (2017).

[10] Umut Gürsoy, Dmitri Kharzeev, and Krishna Rajagopal. "Magnetohydrodynamics, charged currents, and directed flow in heavy ion collisions". In: *Physical Review C* 89.5 (2014), p. 054905.

[11] D Kharzeev. "Can gluons trace baryon number?" In: *Physics Letters B* 378.1-4 (1996), pp. 238–246.

[12] Dmitri E Kharzeev, Larry D McLerran, and Harmen J Warringa. "The effects of topological charge change in heavy ion collisions:"Event by event P and CP violation"". In: *Nuclear Physics A* 803.3-4 (2008), pp. 227–253.

[13] L McLerran and V Skokov. "Comments about the electromagnetic field in heavy-ion collisions". In: *Nuclear Physics A* 929 (2014), pp. 184–190.

[14] Berndt Müller, Jürgen Schukraft, and Bolesław Wysłouch. "First Results from Pb+ Pb collisions at the LHC". In: *Annual Review of Nuclear and Particle Science* 62 (2012), pp. 361–386.

[15] BK Patra et al. "Space–time evolution of ultra-relativistic heavy ion collisions and hadronic spectra". In: *Nuclear Physics A* 709.1-4 (2002), pp. 440–450.

[16] Kirill Tuchin. "Particle production in strong electromagnetic fields in relativistic heavy-ion collisions". In: *Advances in High Energy Physics* 2013 (2013).

[17] Kirill Tuchin. "Synchrotron radiation by fast fermions in heavy-ion collisions". In: *Physical Review C* 82.3 (2010), p. 034904.

[18] Cheuk-Yin Wong. *Introduction to high-energy heavy-ion collisions*. World scientific, 1994.

[19] Yang Zhong et al. "A systematic study of magnetic field in Relativistic Heavy-ion Collisions in the RHIC and LHC energy regions". In: *Advances in High Energy Physics* 2014 (2014).